The 3D effects of a vertical-axis wind turbine

Rotor and wake induction

De Tavernier, D.; Ferreira, C.; Paulsen, U.; Madsen, H.

Important note
To cite this publication, please use the final published version (if applicable).
Please check the document version above.

PAPER • OPEN ACCESS

The 3D effects of a vertical-axis wind turbine: rotor and wake induction

View the article online for updates and enhancements.

IOP ebooks™

Bringing together innovative digital publishing with leading authors from the global scientific community.

Start exploring the collection–download the first chapter of every title for free.

The 3D effects of a vertical-axis wind turbine: rotor and wake induction

D. De Tavernier[1], C. Ferreira[1], U. Paulsen[2], H. Madsen[2]

[1] Delft University of Technology, Wind Energy, Kluyverweg 1, 2629HS Delft, The Netherlands
[2] Technical University of Denmark, Wind Energy, Frederiksborgvej 399, 4000 Roskilde, Denmark

E-mail: `d.a.m.detavernier@tudelft.nl`

Abstract. This paper deals with the 3D effects of a vertical-axis wind turbine caused by the tip vortices. In this study, the VAWT rotor is simplified by the infinitely bladed actuator cylinder concept. The loads are prescribed to be uniform and normal to the surface and are distributed between the upwind and downwind half. Depending on the load configuration, the tip vortices are shed at different locations. This causes the wake induction field and the induction at the rotor to be significantly different. The 3D effects cause a power loss that may go up to 15% depending on the load configuration and aspect ratio. Starting from an aspect ratio of 5, the rotor induction and power is approaching 2D results.

1. Introduction

Although horizontal-axis wind turbines (HAWTs) are widely studied and have proven their technological capabilities, researchers are constantly seeking to lower the cost of energy. For new applications, alternative concepts might show advantages that could be crucial in the search for affordable renewable energy. Vertical-axis wind turbines (VAWTs) might be one of these promising alternatives when considering floating, far-offshore applications. Their lower centre of gravity, omni-directionality and easy scalability make them good candidates.[1] However, they suffer from unsteady loads and fatigue issues. Vertical-axis wind turbines have a long history, though the behaviour of these turbines and its complex flow field is still not fully understood. Advancing the modelling of VAWTs is crucial in order to to evaluate their potential.

So far, limited research is available in literature that is studying the 3D effects of VAWTs. 3D vortex models or CFD models directly include the 3D effects of trailing vorticity, however, in engineering models such as the actuator cylinder model, these 3D effects are not included. Amongst them Paraschivoiu[2], Sharpe[3], Biswas et al.[4] and Beddoes[5] presented tip-effect corrections to represent the finite span effects. However, these approaches are limited since they are applied in a similar way as for HAWTs while the vorticity system of a VAWT is significantly different. As such these models are not capturing the real flow physics of VAWTs. The 3D vortex structures of a VAWT and HAWT are significantly different. It is still rather unclear what the effects are of tip vortices on the rotor and wake induction of a VAWT and to what extend it affects the power generation.

With this motivation, a study is performed to identify the 3D effects of a vertical-axis wind turbine. The focus of this study is two-folded: (1) Understand the vortex system of an actuator

cylinder in 2D and 3D and (2) Identify the 3D effects on the wake induction, the rotor induction and power extraction.

This paper is structured as follows. First, a theoretical description is provided to explain the vortex system of a HAWT and VAWT in 2D and 3D. In section 3, the methodology will be presented. It consist of a description of the modelling techniques used in this study and a model validation. The results and discussion are presented in the next two sections. Section 4 will discuss the wake induction while in section 5, the rotor induction and the effect on the power output is studied. In the final section, we reflect on the research objective of this paper.

2. Vortex system of a VAWT and HAWT

The vorticity equations for incompressible, inviscid flows, as given by Equation 1, states that vorticity can only be created by a change in the force field, i.e. at the locations where the curl of the forcefield is non-zero. As such, you could say that vorticity is a space-dependent parameter. The created vortex lines consequently move with the flow and convect with the local flow velocity.

$$\frac{D\omega}{Dt} = \underbrace{(\omega \cdot \nabla)u}_{=0,\text{no stretching}} - \underbrace{\omega(\nabla \cdot u)}_{=0,\text{incompressible}} + \underbrace{(\nu\nabla^2\omega)}_{=0,\text{inviscid}} + \nabla \times f = \nabla \times f \tag{1}$$

To compare the vortex system created by a HAWT and a VAWT, consider the infinite-bladed simplifications in 2D and 3D: the actuator disk and actuator cylinder respectively. The actuation surface, coinciding with the swept surface of the rotor, is loaded with the average blade forces.

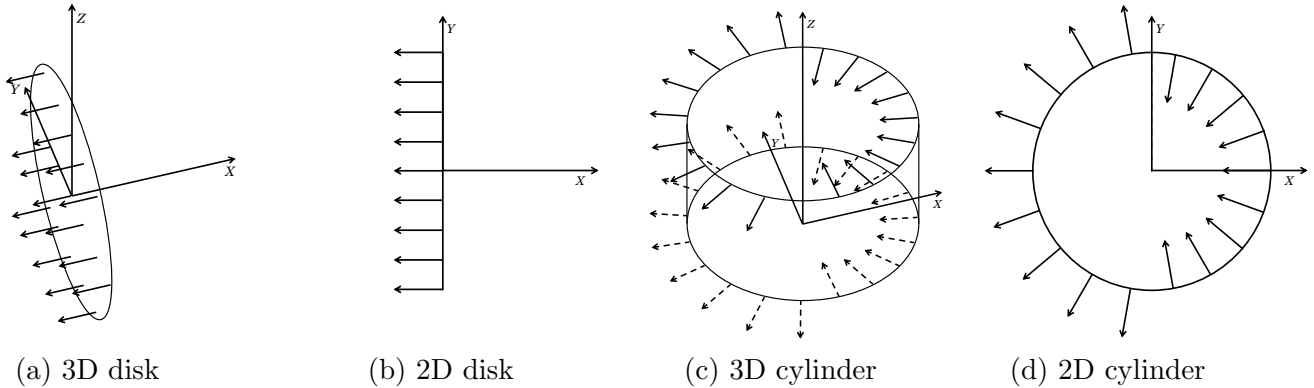(a) 3D disk   (b) 2D disk   (c) 3D cylinder   (d) 2D cylinder

Figure 1: HAWT and VAWT actuation surface in 2D and 3D.

For simplicity, consider a uniformly normal loaded actuator disk in cylindrical coordinates: radial r, azimuthal θ and inflow x-direction. Since the forces are only pointing in x-direction and constant in azimuthal direction, the curl of the forcefield can be simplified to Equation 2. This expression says that only vorticity is created in azimuthal direction. The term df_x/dr is only non-zero at the edges of the disk and thus only vorticity is created there. In 3D, this will lead to the creation of the so-called vortex rings. As an analogy, you could refer to these vortices as tip vortices. For a non-uniformly loaded actuator disk, vorticity will also be shed at different elements inside the rotor but only in the azimuthal direction.

$$\frac{D\omega}{Dt} = \nabla \times f = \begin{bmatrix} \frac{1}{r}\frac{df_x}{d\theta} - \frac{df_\theta}{dx} \\ -\frac{df_x}{dr} + \frac{df_r}{dx} \\ \frac{df_\theta}{dr} - \frac{1}{r}\frac{df_r}{d\theta} \end{bmatrix} = \begin{bmatrix} 0 \\ -\frac{df_x}{dr} \\ 0 \end{bmatrix} \tag{2}$$

The vortex system created by an actuator cylinder is somewhat different. Consider an actuator cylinder with a prescribed uniform load normal to the surface upwind and a uniform load normal to the surface downwind in the direction against the wind. We again use cylindrical coordinates but now defined as: radial r, azimuthal θ and spanwise z-direction. The curl of the force field simplifies to Equation 3 since the forces are zero except in radial direction.

$$\frac{D\omega}{Dt} = \nabla \times f = \begin{bmatrix} \frac{1}{r}\frac{df_z}{d\theta} - \frac{df_\theta}{dz} \\ -\frac{df_z}{dr} + \frac{df_r}{dz} \\ \frac{df_\theta}{dr} - \frac{1}{r}\frac{df_r}{d\theta} \end{bmatrix} = \begin{bmatrix} 0 \\ \frac{df_r}{dz} \\ -\frac{1}{r}\frac{df_r}{d\theta} \end{bmatrix} \tag{3}$$

In 2D, df_r/dz vanishes out and thus the curl of the forcefield is only non-zero in the z-direction at the edges when going from the upwind to the downwind half of the rotor ($df_r/d\theta \neq 0$). As such vorticity will be created at these points only. The strength of the vortex corresponds to the jump made in the load. Note that this vortex structure is exactly the same as the vortex structure created by the 2D actuator disk and that it is independent on how the loads are distributed between the upwind and downwind half.

In 3D, df_r/dz will no longer vanish and is non-zero at the top and bottom of the cylinder. This causes an extra creation of vorticity around the azimuthal direction. For a non-uniformly loaded actuator cylinder (both in spanwise or azimuthal direction), also vorticity would be shed at other elements. To clarify this further, the vortex system of a uniformly loaded actuator cylinder with hypothetically all loads upwind and all loads downwind (with a fixed convecting velocity) is provided in Figure 2. The 3D vortex system including vorticity around the azimuthal- and z-direction is no longer the same when redistributing the loads between the upwind and downwind half although this was true in 2D. The creation of these 3D vortex systems will cause the rotor and wake induction to be different than the 2D case.
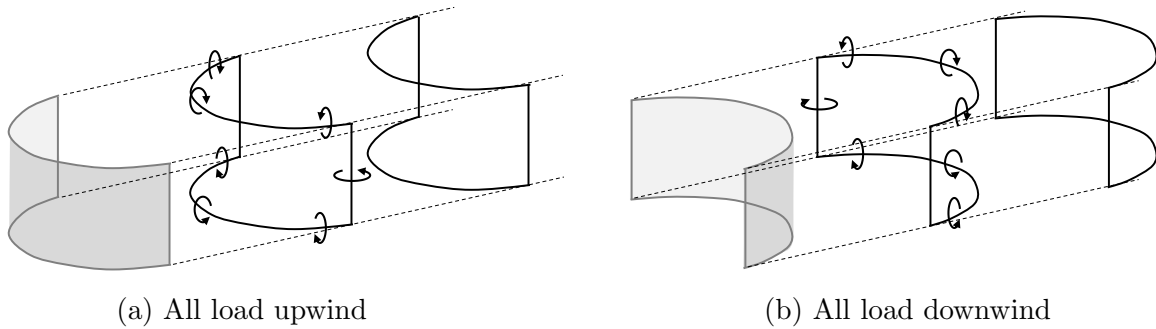

(a) All load upwind   (b) All load downwind

Figure 2: The vortex system of a uniformly normal loaded actuator cylinder with (a) all load upwind and (b) all load downwind.

De Vries[6] and Ferreira[7] explain the vortex system of a finite-bladed HAWT and VAWT by using the lifting line model representation of an aerodynamic wing or any lifting body.[8] For a HAWT, the wake is composed out of trailing vorticity since in steady conditions, the bound vorticity is constant in time. The dominating trailing vortex results from the finite span of the blade. The strength of the wake is determined by the total bound circulation on the blades. The wake of a VAWT, on the other hand, is mainly a result of shed wake vorticity since the bound circulation is constantly changing during rotation. The strength of the wake is in this case determined by the gradient of the bound vorticity. In 2D, the trailing vorticity is neglected, however, in 3D these vortices, and in particular the tip vortices, are playing an important role.

3. Methodology
3.1. Modelling technique
This work mainly focuses on the induction field of an actuator cylinder. The 3D effects will be studied and compared with the 2D results. The velocity field around the 2D and 3D actuator cylinder is modelled using OpenFOAM[9]. A steady-state solver for incompressible flows is used, namely simpleFOAM. The predefined thrust coefficient is realized by introducing distributed volume forces over the actuator cylinder region in the flow. An extra source term is added to the momentum equation of the solver. Simulations are performed for laminar flows and ran till a converged solution is found. Because of symmetry (valid for uniform inflow, no shear), only

the upper part of the 3D rotor is included into the simulations. The domain has size [-40D, 50D] in streamwise direction, [-40D, 40D] in crossflow direction and [0H, 6H] in spanwise direction where D refers to the rotor diameter and H to the blade length. The grid is constructed using BlockMesh and is decomposed into a set of hexahedral cells. The grid is dense around the actuator and gradually becomes more coarse away from the actuator. This mesh has shown to produce converged results for the induction in the wake and at the rotor.

For validation purposes, the open-source actuator line model *TurbineFoam* [10] in OpenFOAM[9] is used. This model is validated intensively in literature and allows to compute the velocity field around a 3D finite-bladed rotor. The model is based on the classical blade element theory and uses the pisoFOAM solver to solve the flow field in space and time. The blades are represented as lines for which the 2D profile lift, drag and pitching moment are input. The loads are again introduced as volume forces to the flow field. No turbulence model is considered. The *TurbineFoam* library includes modules to account for unsteady effects such as dynamic stall, added mass and flow curvature[11]. For simplicity this is not considered in this work since the interest is mainly focussed on the relation between loading and induction and not necessarily in the accurate modelling of a VAWT turbine. The grid contains 17.5 cells per diameter length. Around the rotor and in the turbulent zone, a first order refinement of the mesh is applied. The simulations are run for at least 30 revolutions with a time step every 1 deg azimuthal change. This has shown to produce a converged solution for the turbine loading and wake induction. The power coefficient variation remained below 0.001.

3.2. Model validation

The validation of the OpenFOAM model for the actuator cylinder concept consists of two steps: validate the rotor induction and validate the wake induction.
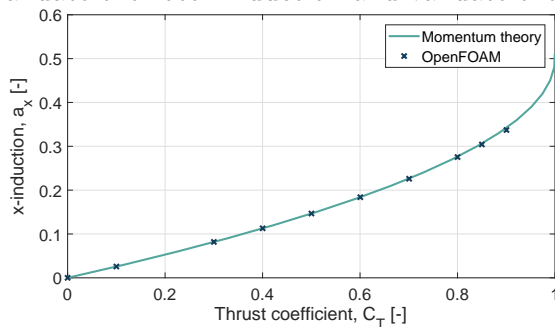
Figure 3: The x-induction at the centre of the AC vs. the thrust coefficient from OpenFOAM model and momentum theory.
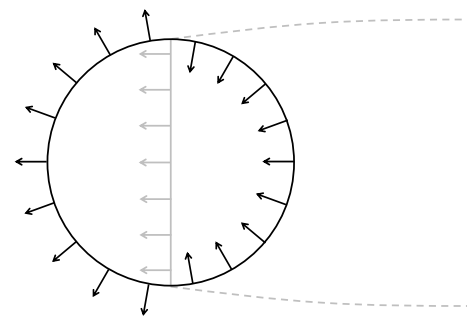
Figure 4: Illustration of the shed vorticity system of a uniformly loaded actuator disk and cylinder.

For the validation of the rotor induction, a 2D actuator cylinder is considered with a uniform normal load pointing outwards applied on the upwind part and a uniform normal load pointing inwards applied on the downwind part. In Figure 3, a comparison of the x-induction at the midpoint of the rotor is presented as a function of the thrust coefficient. This trend is expected to comply with the momentum theory since a uniformly loaded actuator cylinder is creating the same vortex system as an actuator disk, as illustrated in Figure 4. A similar discussion is provided in [12]. The CFD model agrees well with momentum theory for low thrust. The discrepancy of the induction at the centre of the actuator cylinder is slightly larger for the higher thrust values, with a maximum of 1.5%, though still acceptable. The results are also compared to the 3D actuator cylinder for various aspect ratios. At large aspect ratios, the induction at the centre of the actuator cylinder is approaching the 2D results.

The implementation of the OpenFOAM model is also validated by considering the 3D wake induction calculated by the actuator line implementation in OpenFOAM. For this validation purpose, the non-uniform loading of a reference turbine (found by the actuator line model) is

projected as average loading on the actuator cylinder. The magnitude of the loads in both normal and tangential direction are non-uniform with respect to the azimuth and spanwise position.

The reference finite-bladed VAWT has a rotor solidity of 0.085 and a tip speed ratio of 3. The rotor has 3 blades and the blade element characteristics are prescribed by $C_l = 1.11 \cdot 2\pi \cdot sin(\alpha)$ and $C_d = 0$, to represent the characteristics of an 18% inviscid airfoil. The overall thrust coefficient C_T of this turbine is 0.67, the overall tangential force coefficient C_τ is 0.18 according to the actuator line model. The load distribution as a function of the span and azimuth position is given by Figure 5. An azimuth angle from 0 to 180 degrees refers to the upwind half while the azimuth angle from 180 till 360 degrees is the downwind half.

The wake of the finite-bladed VAWT calculated by the actuator line model and the wake behind the infinite-bladed VAWT calculated with the actuator cylinder model are provided in Figure 6. Both wakes show a very similar behaviour however, the roll-up behaviour is slightly more pronounced in the infinite-bladed case. These differences could be contributed to the fact that in the actuator cylinder model the effect of finite number of blades is eliminated. The loads can be shifted more upwind or downwind by introducing a fixed-pitch angle to the blades. This causes the loads to be redistributed between both turbine halves. Similar differences are found when comparing the finite-bladed and infinite-bladed VAWT.

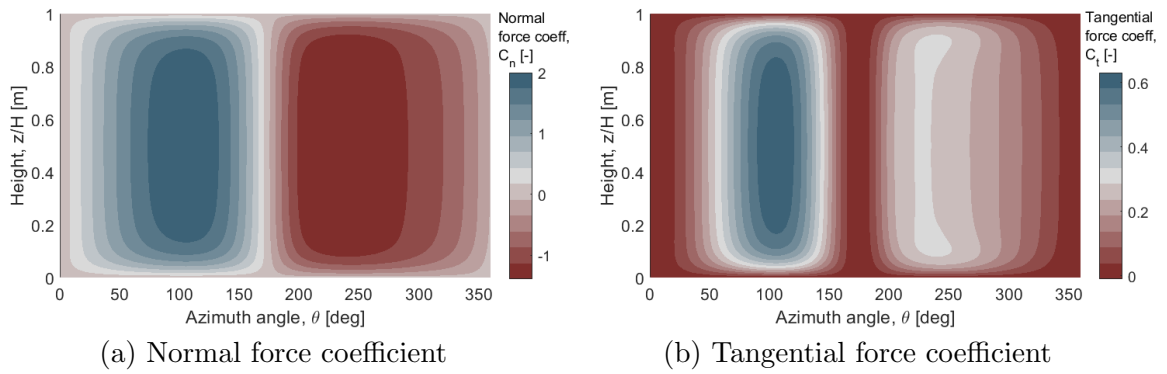(a) Normal force coefficient   (b) Tangential force coefficient

Figure 5: The normal and tangential load coefficient for a finite-bladed VAWT vs. azimuth angle and span height. The rotor solidity is 0.085, the tip speed ratio is 3. $C_l = 1.11 \cdot 2\pi \cdot sin(\alpha)$ and $C_d = 0$.
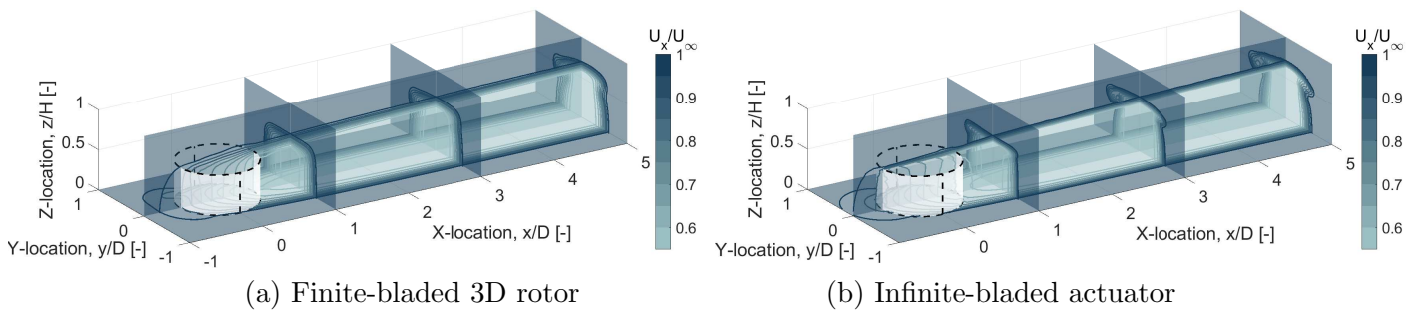

(a) Finite-bladed 3D rotor   (b) Infinite-bladed actuator

Figure 6: X-velocity in the wake behind (a) a finite-bladed 3D rotor and (b) an infinite-bladed actuator cylinder. C_T is 0.67. H/D is 1.

4. Wake induction
4.1. Effect of rotor loading
Consider an actuator cylinder that is uniformly loaded normal to the surface (against the direction of the wind) with a prescribed thrust coefficient. This could be for example an actuator cylinder with all load upwind, an actuator cylinder with all load downwind or the load distributed between the upwind and downwind part. Although these loadings are hypothetical, shifting the loading may be realised in reality by applying a fixed blade pitch angle.
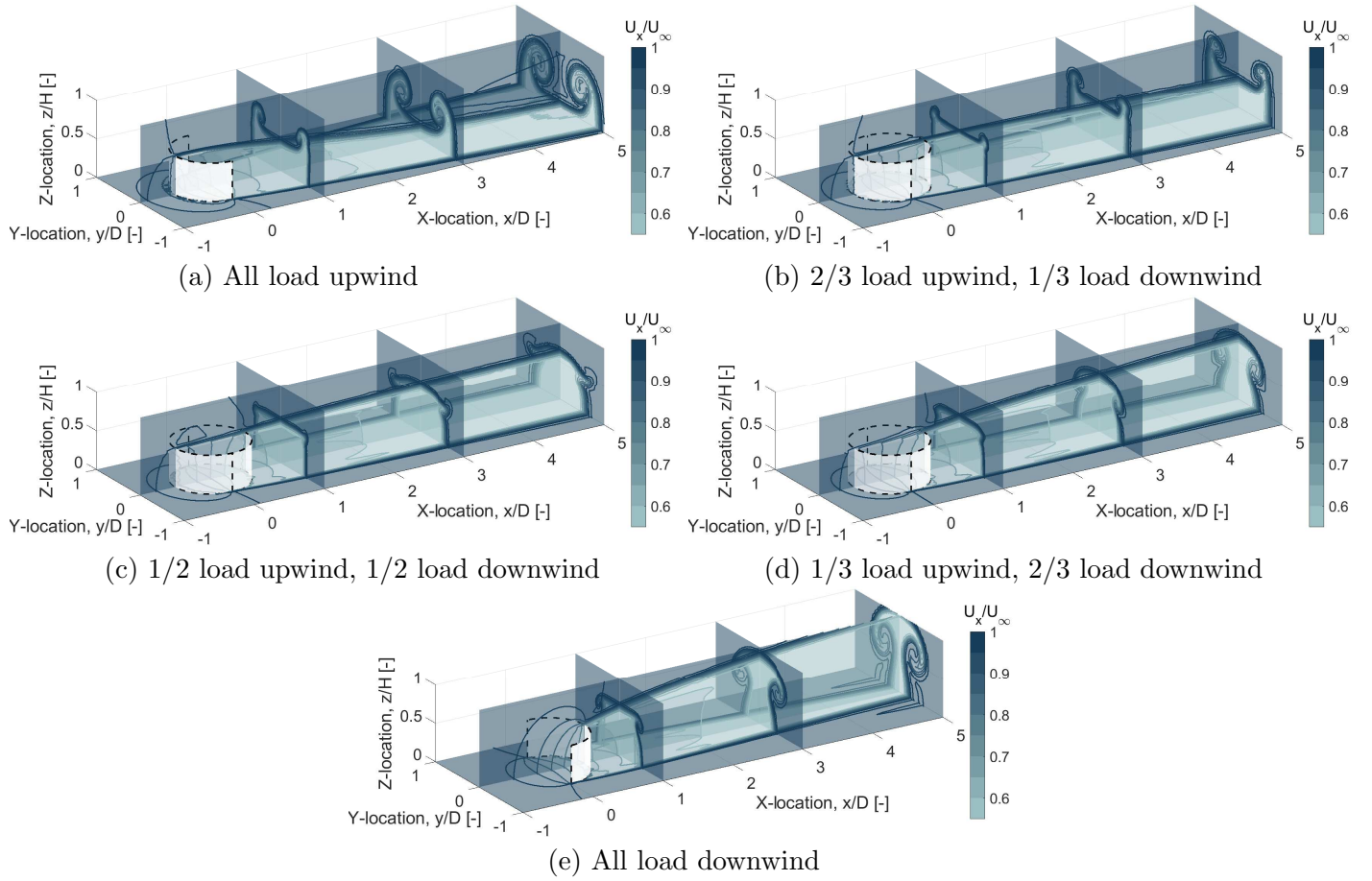
(a) All load upwind

(b) 2/3 load upwind, 1/3 load downwind

(c) 1/2 load upwind, 1/2 load downwind

(d) 1/3 load upwind, 2/3 load downwind

(e) All load downwind

Figure 7: X-velocity in the wake behind a rotor with various load configurations. C_T is 0.67. H/D is 1. The loads are uniform and normal to the actuator.
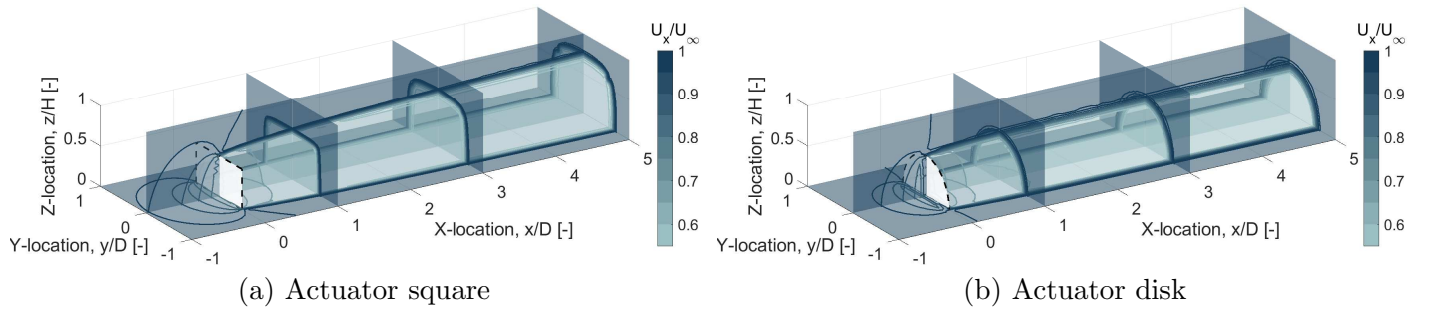

(a) Actuator square

(b) Actuator disk

Figure 8: X-velocity in the wake behind (a) an actuator square and (b) an actuator disk. C_T is 0.67. H/D is 1. The loads are uniform and normal to the actuator.

As already explained, the vorticity field and thus the velocity field will be identical in 2D for all uniformly loaded actuator cylinders with the same thrust coefficient, independent on how the loads are distributed between the upwind and downwind part. Only vorticity is shed at the points where switching from the upwind to the downwind part.

However, in 3D this is no longer the case. In 3D, trailing vorticity appears. In case of a uniformly loaded actuator, these trailing vortices are only located at the top and bottom of the actuator surface around the azimuthal direction, and often referred to as tip vortices. The presence of these tip vortices will cause the vorticity field and thus the velocity field to be significantly different when considering various load configurations. The trailing vortices are shed at various locations, causing the wake characteristics to be different. In case all the load

is located at the upwind part of an actuator cylinder, the trailing vortices cause a re-energising of the wake by pushing the flow from above (and below) inside the wake. In case all load is concentrated downwind, the trailing vortices are pushing the flow from cross-flow direction inside the wake. A clear roll-up is visible when moving further downstream. When the load is distributed between the upwind and downwind part of the rotor, both effects are combined. In Figure 7, the wake of various load configurations is provided.

As a reference, the wake behind a 3D actuator square and actuator disk are provided in Figure 8. Both actuators are again uniformly loaded, normal to the surface against the direction of the wind. The actuator square could be seen as a streamwise projection of the actuator cylinder. In this case, the aspect ratio is 1 and thus the height and width are equal. One diameter behind an actuator square, the wake still shows a square-like shape. When moving further downwind, the shed and trailing vorticity cause the wake to evolve toward a clover shape. For higher thrust coefficients, this behaviour is more pronounced. The actuator disk corresponds to the actuator representation of the HAWT. Behind the actuator disk, vortex rings are shed. The wake profile remains circular but the radius expands moving downstream. Note that the uniformly loaded actuator square and actuator disk would show exactly the same wake as the uniformly loaded actuator cylinder when considering the problem in 2D.

4.2. Effect of aspect ratio

By increasing the aspect ratio, the trailing vortices are located further away from the centre of the rotor. As such the 3D effects may be reduced and the mid-plane could be assumed to be close to 2D. In Figure 9, the x-velocity in a plane three diameters behind the rotor is visualised for an aspect ratio H/D equal to 0.5, 1 and 5. Three rotor loadings are considered: all loads upwind, all load downwind and the loads equally distributed between the upwind and downwind part. Still the rotor is uniformly loaded normal to the actuation surface. For an aspect ratio of 0.5, the wake is clearly 3D and significantly different for the various loadings. When increasing the aspect ratio to 5, one could argue that at the midplane ($z/H = 0$) the wake profiles are rather similar for all three load configurations. The 3D effects are concentrated at the rotor edge (around $z/H=0.5$). Also, the 3D effects are smaller in case the loads are distributed between the upwind and downwind part than in case all loads are concentrated on one half of the actuator cylinder.

5. Rotor induction

Because the wake behind various 3D actuation surfaces is significantly different, it can be expected that the induction at the actuation surface itself is clearly showing 3D effects as well. In Figure 10 the induction at the rotor for three loading configurations is presented: Figure 10 (a-c) shows the induction when all load is concentrated upwind, Figure 10 (d-f) corresponds to the case where the load is equally distributed between the upwind and the downwind half and Figure 10 (g-i) has all loads downwind. The induction is presented as the difference between the 3D and 2D case and normalised with respect to the 2D x-induction at the centre of the rotor (momentum theory). Note that for an aspect ratio of 5, the difference between the 2D and 3D induction tends to zero. However, at lower aspect ratios, the 3D normal induction varies up to 50% from the 2D induction. The largest deviations are identified at the edge of the rotor, while the centre of the rotor converges quicker to the 2D results. Although that no results are provided for other thrust coefficients, calculations confirmed that the same trends are identified for other thrust coefficients.

Changes in the rotor induction for a similar loading case indicate a change in power coefficient. The extracted power of the actuator is defined as the integral over the actuator surface of the normal velocity times the normal loading. As such all red areas in Figure 10 indicate a local power loss while blue areas indicate a power gain. For the upwind and downwind rotor, most of the rotor is coloured red, saying that almost all parts are causing a power loss. For the

upwind/downwind configuration it becomes clear that the upwind part benefits from the 3D effect, while the downwind part suffers from 3D effects in terms of power coefficient.
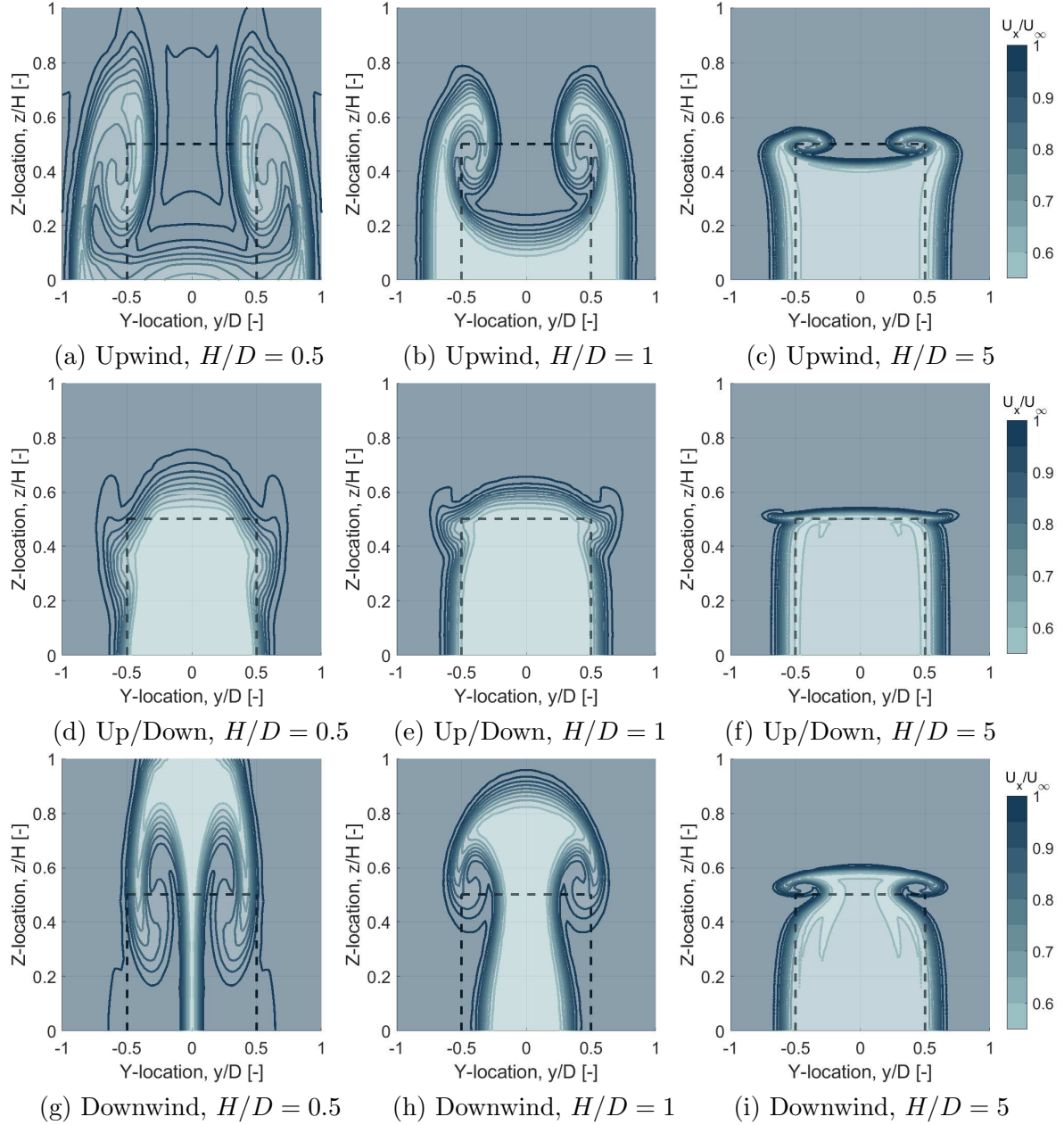

Figure 9: X-velocity in the wake-plane 3 diameters behind the centre of the rotor for various load configurations. C_T is 0.67. H/D is 0.5, 1 or 5. The loads are uniform and normal to the actuator.

In Figure 11, the loss in power for various combinations of rotor loadings and aspect ratios is quantified. Note that the configurations with all load upwind or all load downwind show the highest power loss. Also from the wake plots, it was already clear that these cases showed the most 3D wake. In case the load is distributed between the upwind and downwind half, the wake behaved in a more 2D matter and this result is also recognised in the power loss. For an aspect ratio of 5, the power loss remains below 1%. This could suggest that neglecting tip effects or using a 2D model might be appropriate for further analysis. However, for a VAWT with aspect ratio of 0.25, the power loss may go up to 15%. In this case, using 2D modelling techniques are

inapplicable and neglecting tip effects does not provide reliable results.

(a) Upwind, $H/D = 0.5$ (b) Upwind, $H/D = 1$ (c) Upwind, $H/D = 5$

(d) Up/Down, $H/D = 0.5$ (e) Up/Down, $H/D = 1$ (f) Up/Down, $H/D = 5$

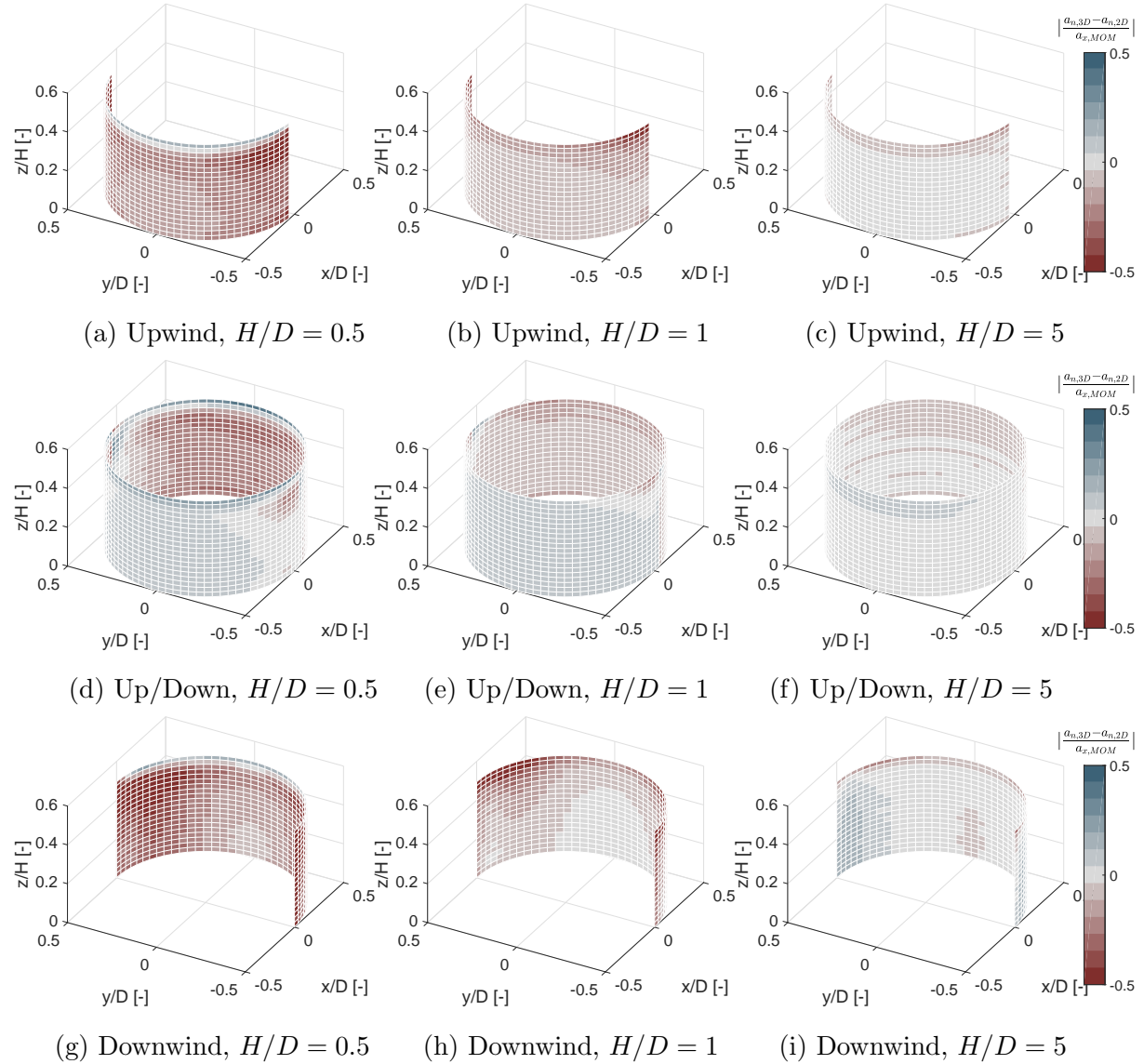(g) Downwind, $H/D = 0.5$ (h) Downwind, $H/D = 1$ (i) Downwind, $H/D = 5$

Figure 10: Difference between the 3D and 2D normal induction for an actuator cylinder normalised with the x-induction according to the momentum theory. A negative sign indicates local power loss, a positive sign indicates local power gain. C_T is 0.67. The loads are uniform and normal to the actuator.

6. Conclusion

Since VAWTs are intrinsically unsteady, the wake of a VAWT mainly consists of shed wake vorticity and the strength is given by the gradient of the bound vorticity. In 3D, also trailing vorticity and in particular the tip vortex plays an important role. This paper investigates the effect of the tip vortex on the wake induction, the rotor induction and the power coefficient.

This study focusses on the infinite-bladed actuator cylinder. The VAWT is simplified to an actuation surface and is loaded with a prescribed load: a uniform load normal to the actuation surface pointing against the incoming wind, in order to mimic the loading of a real VAWT. The loads are distributed between the upwind and downwind half. This simplified load case allows to systematically study the vortex system and helps to understand the basic principles.

The wake study reveals that the load configuration significantly effects the wake. The tip vortices of an actuator that is fully loaded upwind or fully loaded downwind are shed at various

locations and thus the wake characteristics are different. For large aspect ratios ($H/D > 5$), the trailing vortices are located further away from the centre of the rotor and as such the mid-plane is approaching 2D conditions. The 3D effects are concentrated at the rotor edges.

Because the wake behind the 3D actuation surface is indicating 3D effects, also the rotor induction is expected to suffer from the tip vorticity. For an aspect ratio of 5, the difference between the 2D and 3D induction tends to zero. However, at smaller aspect ratios, the 3D normal induction may vary up to 50% from the 2D induction, depending on the rotor loading. The largest 3D effects are indicated at the edges of the rotor. As a result the 3D power extraction may be up to 15% lower than the 2D power extraction. For an aspect ratio of 5, the power loss remains below 1% for all load configurations.

It is expected that in case of finite number of blades the 3D losses will increase since vorticity is concentrated more. This also holds for larger thrust coefficients. A real operational VAWT will most probably approach a load configuration of 2/3 of the load upwind and 1/3 downwind but a redistribution of the loads may be achieved by a fixed blade pitch angle. Finally, most VAWTs that are considered these days have an aspect ratio close to one. This study shows that in these cases, it is of major importance to already include 3D effects early in the design phase since the operational conditions may be significantly different than in 2D.
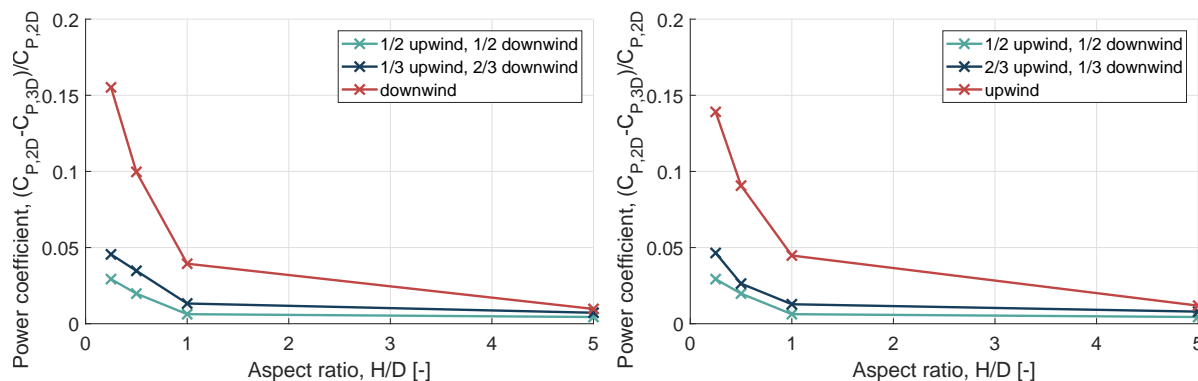

Figure 11: Loss in power coefficient compared to the 2D power extraction for various rotor loadings. C_T is 0.67. The loads are uniform and normal to the actuator.

7. References

[1] U.S. Paulsen, M. Borg, H.A. Madsen, T.F. Pedersen, et al. Outcomes of the deepwind conceptual design. *Energy Procedia*, 80:329–341, 2015.
[2] I. Paraschivoiu. *Wind turbine design with emphasis on Darrieus*. Polythecnic International Press, 2002.
[3] D. Sharpe. Refinements and developments of the multiple stream tube theory for the aerodynamic performance of vertical axis wind turbines. *Proceedings of the Sixth BWEA Wind Energy Conference*, pages 148–159, 1984.
[4] S. Biswas, B.N. Sreedhar, and Y.P. Singh. A new analytical model for the aerodynamic performance analysis of vertical axis wind turbines. *Wind Engineering*, 19(2):107–119, 1995.
[5] T.S. Beddoes. A near wake dynamic model. *Proceedings of the AHS national specialist meeting on aerodynamics and aeroacoustics*, 1987.
[6] O. de Vries. Fluid dynamic aspects of wind energy conversion. Report AGARDograph No. 243, National Aerospace Laboratory NLR, 1978.
[7] C.S. Ferreira. *The near wake of the VAWT*. Phd thesis, Delft University of Technology, 2009.
[8] J.D. Anderson Jr. *Fundamentals of aerodynamics*. McGraw-Hill, fifth edition, 2001.
[9] The OpenFOAM Foundation Ltd. OpenFOAM v6, *https://openfoam.org*. , 2018.
[10] P. Bachant, A. Goude, and M. Wosnik. Turbinesfoam/turbinesfoam: v0.0.8, zenodo, 2018. `http://doi.org/10.5281/zenodo.1210366`.
[11] P. Bachant, A. Goude, and M. Wosnik. Actuator line modeling of vertical-axis turbines. *arXiv*, (1605.01449v4), 2018.
[12] H.A. Madsen, U.S. Paulsen, and L. Vitae. Analysis of VAWT aerodynamics and design using the Actuator Cylinder flow model. *Journal of Physics: Conference Series*, 555:012065, 2014.